Exploiting satellite measurements to explore uncertainties in UK bottom-up NO_x emission estimates

Richard J. Pope[1,2], Rebecca Kelly[1], Eloise A. Marais[3], Ailish M. Graham[1], Chris Wilson[1,2], Jeremy J. Harrison[4,5], Savio J. A. Moniz[6], Mohamed Ghalaieny[6], Steve R. Arnold[1] and Martyn P. Chipperfield[1,2]

1: School of Earth and Environment, University of Leeds, Leeds, UK

2: National Centre for Earth Observation, University of Leeds, Leeds, UK

3: Department of Geography, University College London, London, UK

4: Department of Physics and Astronomy, University of Leicester, Leicester, UK

5: National Centre for Earth Observation, University of Leicester, Leicester, UK

6: Department for Environment, Food and Rural Affairs, 2 Marsham Street, London, UK

Resubmitted to *Atmospheric Chemistry and Physics*

Correspondence to: Richard J. Pope (r.j.pope@leeds.ac.uk)

Abstract

Nitrogen oxides (NO_x, $NO+NO_2$) are potent air pollutants which directly impact on human health and which aid the formation of other hazardous pollutants such as ozone (O_3) and particulate matter. In this study, we use satellite tropospheric column nitrogen dioxide ($TCNO_2$) data to evaluate the spatiotemporal variability and magnitude of the United Kingdom (UK) bottom-up National Atmospheric Emissions Inventory (NAEI) NO_x emissions. Although emissions and $TCNO_2$ represent different quantities, for UK city sources we find a spatial correlation of ~0.5 between the NAEI NO_x emissions and $TCNO_2$ from the high-spatial-resolution TROPOspheric Monitoring Instrument (TROPOMI), suggesting a good spatial distribution of emission sources in the inventory. Between 2005 and 2015, the NAEI total UK NO_x emissions and long-term $TCNO_2$ record from the Ozone Monitoring Instrument (OMI), averaged over England, show annually decreasing trends of 4.4% and 2.2%, respectively. Top-down NO_x emissions were derived in this study by applying a simple mass balance approach to TROPOMI observed downwind NO_2 plumes from city sources. Overall, these top-down estimates were consistent with the NAEI, but for larger cities such as London and Birmingham the inventory is significantly (>25%) less than the top-down emissions.

1. Introduction

Poor air quality (AQ) can have a substantial impact on human health, increasing risk of ailments such as asthma, cancer, diabetes and heart disease (Royal College of Physicians, 2016). A key air pollutant is nitrogen dioxide (NO_2) which was responsible for approximately 9600 premature deaths from long-term exposure in the UK in 2015 (EEA, 2018). NO_2 is also a precursor to tropospheric ozone and nitrate aerosol in the UK (DEFRA, 2018a). Legislation (e.g. the EU directive 2008/50/EC Ambient AQ regulation, (DEFRA, 2018a)) is in place to reduce concentrations of NO_2 and other pollutants. However, many regions in the UK (33 out of 43 in 2019; DEFRA, 2020) still fail to meet the annual mean NO_2 limit of 40 μg/m^3 (WHO, 2018). To meet the UK's statutory reporting requirements and to help inform policy, Defra uses the National Atmospheric Emissions Inventory (NAEI, 2021). However, like all emission inventories, the NAEI is subject to uncertainties which are difficult to quantify. These uncertainties include unreported sources, diffuse sources such as agriculture, the use of proxy data (e.g. population or housing density data) to distribute emissions and updates to the NAEI methodologies between years (NAEI, 2017). In addition, the NAEI only includes emissions from anthropogenic sources. Spatial verification of the NAEI AQ emissions, until recently (Tsagatakis et al., 2021), has been restricted to comparisons with surface sites, which have limited and disproportional spatial coverage. The NAEI is also used to drive regional models (e.g. the UK Met Office Air Quality in the Unified Model (AQUM, Savage et al., 2013) which provides the official national AQ forecasts), land use regression models (e.g. Wu et al., 2017) and Pollutant Climate Mapping (PCM) models (e.g. Dibbens and Clemens, 2015), where uncertainties in the emissions can then feed into the simulated AQ predictions and resultant public health advisories.

Satellite measurements of tropospheric column NO_2 ($TCNO_2$) have frequently been used to derive top-down emissions of nitrogen oxides (NO_x = nitric oxide (NO) + NO_2), which can be used to evaluate bottom-up inventories. Some studies have used statistical fitting of observed downwind plumes of $TCNO_2$ from anthropogenic sources (e.g. Beirle et al., 2011; Liu et al., 2016; Verstraeten et al., 2018), while others have used complex atmospheric chemistry models deploying approaches such as data assimilation (e.g. Miyazaki et al., 2016), mass balance (Martin et al., 2003) and model sensitivity experiments (e.g. Potts et al., 2021).

While model-derived estimates of NO_x emissions (e.g. from data assimilation) are robust, the methodology is computationally expensive and time intensive. Therefore, the statistical fitting to downwind plumes approach is a more achievable approach to derive top-down emissions, especially for government departments and agencies. Beirle et al. (2011) presented one of the first studies to use statistical fitting to downwind plumes for Riyadh, Saudi Arabia. The method was also applied to multiple megacities and compared with the bottom-up Environmental Database for Global Atmospheric Research (EDGAR) emission inventory (version 4.1). Verstraeten et al. (2018) used a similar, but modified, approach of a simple mass balance which assumes that the observed total mass of NO_2 is a product of the emission rate and the effective lifetime. The assumption is that the removal of NO_2 can be described by a first-order loss (i.e. the chemical decay of NO_2 follows an exponential decay function with an e-folding time, and therefore distance from source).

In this study, we use satellite $TCNO_2$ records to evaluate the spatial distribution and temporal evolution of the NAEI. In the past, and still presently, this is a challenge given the climatological meteorological conditions (i.e. frequent frontal systems with widespread precipitation and cloud cover; Pena-Angulo et al., (2020)) experienced in the UK. Frequent cloud cover means that satellite instruments are severely restricted in their ability to retrieve information on trace gases and aerosols through the atmosphere (i.e. retrievals only between the top of atmosphere and cloud top). Therefore, the lack of robust observations makes it more difficult to clearly resolve large emission sources from space. Also, previous sensors (e.g. the Ozone Monitoring Instrument, OMI) have had relatively coarse horizontal spatial resolutions (in the order of 10-100 km) which are larger than most UK emissions sources. However, this work represents the first attempt to derive UK city-scale NO_x emissions from the new state-of-the-art TROPOspheric Monitoring Instrument (TROPOMI), which has unparalleled spatial resolution in comparison to previous sensors (e.g. OMI). We apply a similar approach to Verstraeten et al. (2018), but determine the background NO_2 value and e-folding distance in different ways, to derive top-down NO_x emission estimates of UK cities and thereby directly evaluate the NAEI estimates. Therefore, we can derive NO_x emissions from previously undetectable sources (e.g. Manchester and Birmingham). From here on, we refer to this methodology as the simple mass balance approach (SMBA). The satellite observations used, NAEI and SMBA are described in Section 2, the results presented in Section 3 and our conclusions discussed in Section 4.

2. Data and Methods

2.1 NAEI Emissions

The NAEI is the official UK bottom-up inventory of primary sources of emissions, used for statutory reporting, national air quality policy and driving regional air quality models (NAEI, 2021). The contract to deliver the NAEI is led by a consortium managed by Ricardo Energy and Environment for the UK Department for Business, Energy and Industrial Strategy (BEIS) and the Department for Environment, Food and Rural Affairs (Defra). The NAEI is compiled on an annual basis according to internationally agreed methodologies (EMEP/EEA, 2019), encompassing sectors ranging from transport, industry, through to agriculture and domestic sources (Ricardo Energy and Environment, 2021). Here, we use the NAEI emissions from 2019, which is the most recent version publically available.

2.2 Satellite Data

OMI and TROPOMI are both nadir-viewing instruments on-board the NASA Aura and ESA Sentinel 5 – Precursor (S5P) polar orbiting satellites, respectively, and have local overpass times of 13:30. TROPOMI measures in the ultraviolet-visible (UV-Vis, 270-500 nm), similar to OMI (Boersma et al., 2007), as well as near-infrared (NIR, 675-775 nm) and short-wave infrared (SWIR, 2305-2385 nm) spectral ranges (Veefkind et al., 2012). TROPOMI and OMI have nadir pixel sizes of 3.5 km × 5.5 km (in the UV-Vis, 7.0 km × 7.0 km for other spectral ranges) and 13 km × 24 km, respectively. The OMI (DOMINO version 2 product) and TROPOMI (TM5-MP-DOMINO version 1.2/3x – OFFLINE product) data were downloaded from the Tropospheric Emissions Monitoring Internet Service (TEMIS) for January 2005 to December 2015 and February 2018 to January 2020, respectively. Given the issues with large cloud cover in the UK, we use two years of TROPOMI $TCNO_2$ data to help increase the spatiotemporal sample size when deriving top-down emissions to evaluate the 2019 NAEI NO_x emissions. The OMI row anomaly first occurred in 2008 (Torres et al., 2018) and over time has progressively had a detrimental impact on retrieved $TCNO_2$. The study by Pope et al., (2018) successfully used the OMI record to look at long-term trends in UK $TCNO_2$. However, after 2015, while still retrieving robust signals over source regions, the row anomaly appears to be substantially artificially enhancing background $TCNO_2$. Therefore, as we consider regional trends in $TCNO_2$ in Section 3.2, we did not use OMI $TCNO_2$ after 2015. The data has been processed using the methodology of Pope et al., (2018) to map the $TCNO_2$ data onto a high-resolution spatial grid ($0.025^o \times 0.025^o$, ~2-3 km × ~2-3 km for TROPOMI, $0.05^o \times 0.05^o$, ~5 km × ~5 km for OMI). The TROPOMI data were quality controlled for a cloud radiance fraction <0.5, a quality control flag >0.75 and where the $TCNO_2$ value was > -1.0×10^{-5} moles/m^2 (i.e. random values round 0.0 may be slightly negative or positive so we filter for $TCNO_2$ > -1.0×10^{-5} moles/m^2 otherwise a positive bias in average $TCNO_2$ is imposed). While TROPOMI provides the greatest spatial resolution of any satellite instrument to measure air pollutants, suitable to derive $TCNO_2$ emission estimates over UK city-scale sources, the retrieved $TCNO_2$ has been shown to have a low bias. Over north-western Europe, Verhoelst et al., (2021) found that TROPOMI underestimated $TCNO_2$ by approximately 20-30% when compared with surface $TCNO_2$ measurements, which is consistent with Chan et al., (2020) and Dimitropoulou et al., (2020). OMI data were processed for a geometric cloud fraction of <0.2, quality flag = 0 (which also flags pixels influenced by the row anomaly (Braak, 2010)) and $TCNO_2$ > -1.0×10^{-5} moles/m^2.

2.3 Simplified Mass Balance Approach

To derive top-down emissions of NO_x we use the SMBA, which is based on downwind plumes of TROPOMI observed $TCNO_2$ from the target source where the observed total mass of NO_2 (i.e. the source-related enhancement of $TCNO_2$ above the background level) is assumed to be a product of the emission rate and the effective lifetime. Therefore, we can derive the NO_x emission rate based on **Equation 1**:

$$E = \frac{\sum_{i=0}^{N}((NO_2\ LD_i - B\ LD) \times\ \Delta d_i)}{t\ \times e^{\frac{-t}{\tau}}} \times f \tag{1}$$

where E is the emission rate (moles/s), $NO_2\ LD$ is the NO_2 line density (moles/m), $B\ LD$ is the background NO_2 line density value (moles/m), Δd is the grid box length (m), i is the grid box number between the source and background value, t is time (s) and $e^{\frac{-t}{\tau}}$ is the e-folding loss term with τ as the effective lifetime. N represents the number of satellite $TCNO_2$ grid boxes between the source and background level B. t is calculated as the distance between the source and B divided by the wind speed (*ws*). To derive the full NO_2 loading emitted from the source, the wind flow $NO_2\ LD$ has the background $NO_2\ LD$ (i.e. $B\ LD$) value subtracted from all points between the source and B and is then summed yielding the total NO_2 mass (moles). f is the factor required to convert to NO_x emissions.

The wind speed and direction at a particular source are determined from the European Centre for Medium-Range Weather Forecasts (ECMWF, 2021) ERA5 u- & v-wind component data. The wind data are sampled at 13:00 UTC (around 13:00 local time (LT) over the UK) to coincide with the TROPOMI overpass (i.e. 13:30 LT) and averaged across boundary layer pressure levels (i.e. surface to 900 hPa). In all cases, the *ws* had to be greater than 2 m/s to avoid near stable meteorological conditions. Wind data is only used on days where there is TROPOMI NO_2 data available downwind of the target source, when deriving the average directional wind speed. Studies such as Beirle et al. (2011) and Verstraeten et al. (2018) averaged the wind speeds over the surface to 500 m layer. Beirle et al. (2011) suggested that the average winds across this altitude range yielded uncertainties over approximately 30%, but neither study provided definitive reasoning why 500 m was selected. In the UK, 500 m is approximately 950 hPa which sits comfortably within the boundary layer (approximately 1000 m or 880.0 to 910 hPa in **Figure 1a** based on ERA-5 data sampled at 13.00 LT and averaged for 2019). In this study, we argue that wind speeds throughout the boundary layer are likely to be important in controlling the spatial distribution of NO_2 downwind of sources. **Figure 1b** shows the zonally averaged latitude-pressure NO_2 profile from the Copernicus Atmosphere Monitoring Service (CAMS, 2021), sampled at 13.00 LT and averaged for 2019, over the UK. The bulk of the NO_2 loading is near the surface with NO_2 concentrations of 0.5 ppbv to >1.0 ppbv between the surface and 900 hPa. As shown by the white dashed lines, 60-70% of the surface to 500 hPa NO_2 loading exists between the surface and 900 hPa. The zonally averaged boundary layer pressure (red dashed line) also straddles the 900 hPa level. In **Figure 1c**, the wind speed profile for London sampled under westerly flow increases with altitude until between 925 hPa and 900 hPa. For each pressure level, London westerly days are defined based average u- and v-components between the surface and the respective pressure level. As shown by the blue text, the wind speed gradient with respect to pressure substantially decreases (i.e. from -0.0406 m/s/hPa between 950 hPa and 925 hPa to -0.0045 m/s/hPa between 925 hPa and 900 hPa) at 900 hPa. Therefore, this profile gradient and the information in **Figures 1a** & **b** suggest that 900 hPa is a suitable level to derive the boundary layer average wind speed and flow direction. The table (**panel d**) in **Figure 1** shows the sensitivity of the NO_x emission parameters to the pressure layer used. The derivation of emissions is discussed further in this section. The surface-850 hPa average and surface only winds show substantially different NO_x emission rates of 61.6 moles/s and 30.1 moles/s, respectively. However, the intermediate levels (900 hPa and 950 hPa) show less dramatic step changes with emission rates of 55.2 moles/s and 49.8 moles/s. Therefore, the surface-900 hPa layer is used to help derive NO_x emission rates in this study.

The *NO_2 LD* is the product of the source width, which is perpendicular to the wind flow, and the source-width-average $TCNO_2$ (i.e. for each downwind grid box from the source, the corresponding perpendicular rows between the source edges are averaged together) profile downwind from the source on a grid box by grid box basis as shown in **Equation 2**.

$$NO_2LD_{i=1,N} = \frac{\sum_{j=1}^{n} TCNO_{2i,j}}{n} \times w \qquad (2)$$

where *NO_2 LD* (moles/m) is the NO_2 line density, *i* the grid box index downwind of the source starting at *i=1* going to *i=N* at background point *B*, *$TCNO_2$* is the tropospheric column NO_2 grid box value (moles/m^2) at point *i* and *j* is the grid box index for the number of grid boxes *n*, perpendicular to the downwind profile, which fit across the width of the source at grid box *i* downwind and *w* is the source width (m) (i.e. source width perpendicular to the downwind profile) of the NO_2 source. Though the source width and length are subjective choices between the source edge locations, the same source width and length values are used when deriving the TROPOMI NO_x emissions and summing up the NAEI NO_x emissions over the source region. As the source emissions will be a function of the source width (i.e. larger at source centre and lower at source edge), the mean $TCNO_2$ downwind profile is representative of the source-average NO_2 emission.

Figure 2a shows the difference between TROPOMI $TCNO_2$ sampled under westerly flow and the long-term average based on London u- and v-wind components, where there are clear downwind positive anomalies >3.0×10^{-5} moles/m^2. Similarly in **Figure 2b**, the downwind plume (e.g. westerly flow over London) has typically larger *NO_2 LD* values than the all-flow (i.e. all wind directions) *NO_2 LD*. The full NO_2 mass emitted from the source in the *NO_2 LD* is the summation of the wind-flow *NO_2 LD* from source up to point *B* minus the background value from all downwind pixels over this profile segment. A reasonable estimate of when the wind-flow *NO_2 LD* reaches *B*, for more isolated NO_2 sources, is when it intersects with the all-flow *NO_2 LD* profile (i.e. returns to normal levels). However, when there are substantial upwind NO_2 sources, this can yield wind-flow *NO_2 LD* profiles which never intersect with the all-flow *NO_2 LD* profile within the domain (e.g. see Birmingham example in **Figure 3a & b**). Therefore, to determine when *B*, in the downwind direction, has been reached, a running t-test was applied to the wind-flow *NO_2 LD* profile to determine where turning points or levelling off occurred. Such a substantial change in the *NO_2 LD* profile gradient is indicative of the background level being reached and/or potentially another source being identified (e.g. in **Figure 2b** there is evidence of other NO_2 sources downwind of London several hundred kilometres away over continental Europe). As such a test can be sensitive to noise in the $TCNO_2$ data, a 10-pixel (0.5°) running average wind-flow *NO2 LD* profile was calculated. This smoothed out the noise from the downwind profile and allowed for the detection of larger-scale *NO_2 LD* changes. The running t-test was applied to this using two windows (i.e. a moving centre point with a window each side of 0.5°) and the t-test significance between the two window averages determined. This yielded a t-test significance/p-value distance series from the source. When a substantial change in the *NO_2 LD* gradient occurred, the t-test p-values values would increase, peak and then drop off. This change in the gradient of the t-test p-values identified the location of any *NO_2 LD* step changes in the profile. The green line in **Figure 2b** shows where the t-test p-values peaked and that there are turning points in the wind-flow *NO2 LD* profile. Such a reduction in the wind-flow *NO_2 LD* profile gradient is suggestive of the plume reaching *B* as NO_2 levels have stabilised. However, in **Figure 2b**, there are multiple locations potentially meeting this criteria. In reality, the turning points further downwind of London are sources from the Benelux region. The red dot represents the first instance, after the initial near-source wind-flow *NO2 LD* peak, where the gradient in the running t-test p-value profile changes sign (i.e. positive to negative or vice versa).

The loss term $e^{\frac{-t}{\tau}}$ is dependent upon τ and is determined by applying an e-folding distance fit between the near-source peak wind-flow *NO_2 LD* value and *B* (i.e. we assume this function is valid only between these two points), before dividing by *ws* to get τ. Here, a range of e-folding distances are tested in the loss term $e^{\frac{-t}{\tau}}$ to find the distance value which yields the lowest root mean square error (RMSE), and a large R^2 (Pearson correlation coefficient squared) value, between the e-folding distance fit (red line, **Figure 2c**) and the wind-flow *NO_2 LD* (black line, **Figure 2c**). In the case of London, this yielded an e-folding distance of 148.0 km and τ of 4.5 hours (4.7 and 4.3 hours) based on the average *ws* = 9.1 m/s with an uncertainty range (± 0.4 m/s; i.e. ± 1-sigma standard error) of 8.7 m/s to 9.5 m/s (i.e. a slower/faster wind speed yields a longer/shorter lifetime). The effective lifetime derived here for London and other UK cities is typically consistent with values from other studies (e.g. Beirle et al., (2011) and Verstraeten et al. (2018)) for European cities (i.e. 1.0 –10.0 hours).

The top-down E is calculated from **Equation 1** and this emissions flux of NO_2 (moles/s) is converted to emissions of NO_x (moles/s) using the factor f for comparison with the bottom-up inventories. This is done by scaling the NO_2 emissions by 1.32 based on the NO:NO_2 concentration ratio (0.32) in urban environments at midday (Seinfeld and Pandis, 2006; Liu et al., 2016). Verstraeten et al., (2018) used modelled NO and NO_2 concentrations to derive a scaling more representative of the chemistry of the source. They estimate there is a 10% uncertainty (similar to Beirle et al., (2011)), but as the modelled NO_2:NO_x ratio is based on the input emissions, for which the satellite data is being used to evaluate, this process is rather circular and not independent.

Here, the top-down NO_x emissions are derived by sampling $TCNO_2$ data under different wind directions in all seasons. Several studies, such as Beirle et al. (2011), have gone a step further and used $TCNO_2$ data to derive seasonal emissions. Unfortunately, here we are restricted to looking at annually derived emissions due to 1) the TROPOMI $TCNO_2$ record only started in February 2018, 2) the COVID-19 pandemic resulted in a dramatic reduction in UK (and global) NO_x emissions (Potts et al., 2021) meaning $TCNO_2$ data beyond February 2020 could not be used to derive top-down emissions under normal conditions and 3) the UK is subject to frequently cloudy conditions yielding a reduction in the number of observations from TROPOMI. The latter point predominantly influences TROPOMI retrievals in the winter-time. Therefore, even though we sample $TCNO_2$ data in all seasons, there is likely to be a tendency towards summer-time $TCNO_2$ values, when $TCNO_2$ values tend to be lower (e.g. Pope et al., 2015), potentially leading to a low bias in the derived top-down NO_x emissions.

To investigate the total errors in the derived NO_x emissions from TROPOMI, we have included errors from all the input terms. These include the enhancement in the $TNCO_2$ data, the e-folding distance x_o, the wind speed ws, the source width w, the NO_2 to NO_x conversion factor f and the distance d between the source and B. When combined, this yields the total error in Equation 3:

$$\Delta E = E\sqrt{\frac{\Delta\phi^2}{\phi^2} + \frac{\Delta ws^2}{ws^2} + \frac{\Delta w^2}{w^2} + \frac{\Delta f^2}{f^2} + \frac{d^2}{x_o^2}\left[\frac{\Delta d^2}{d^2} + \frac{\Delta x_o^2}{x_o^2}\right]} \qquad (3)$$

In the total error expression, we have set $\phi = \overline{NO_2} - B$, where $\overline{NO_2}$ is the average $TCNO_2$ value (moles/m^2) for all grid cells between the source and B (i.e. background $TCNO_2$ value) in the downwind profile. Here, we take $\phi \times d \times w$ to be a suitable estimate of the full NO_2 emission loading from the source (i.e. the numerator of Equation 1). Regarding the errors (i.e. terms with Δ in front), based on Beirle et al., (2011), we assign errors of 10% to f and w. As x_o and d are distance metrics as well, with no clear way to quantify the errors in these terms, we have assigned them with 10% errors also. The ws error is based on the standard error in the sample (i.e. the number days selected for each flow regime). For the enhancement in $TCNO_2$ from the source (i.e. ϕ), we have conservatively taken the largest precision error value from all $TCNO_2$ values between the source and B, which forms $\overline{NO_2}$.

3. Results

3.1 NO_x Sources

Surface emissions and observed $TCNO_2$ represent different quantities and are influenced by different processes. However, the short NO_2 lifetime of a few hours (Schaub et al., 2007; Pope et al., 2015) means there is a sharp gradient between sources and the background levels. Therefore, we can use the satellite $TCNO_2$ observations to provide some constraint on the spatial distribution of the NO_x emissions. In **Figure 4**, spatial maps over south-eastern (**Figure 4a & c**) and northern England (**Figure 4b & d**) show evidence of co-located $TCNO_2$ and NO_x emission hot spots, especially over many of the UK cities shown by circles. Here, both data sets have been mapped onto the spatial resolution of $0.025^o \times 0.025^o$. In South East England, $TCNO_2$ and NO_x emissions peak over London at over 14.0×10^{-5} moles/m^2 and approximately >2.0 μg/m^2/s, respectively. A secondary peak is also observed over western London for both quantities at similar levels. There are further co-located hotspots over Southampton ($TCNO_2$ ~8.0-9.0×10^{-5} moles/m^2, NO_x >2.0 μg/m^2/s), Portsmouth ($TCNO_2$ ~6.0-7.0×10^{-5} moles/m^2, NO_x ~1.0-1.5 μg/m^2/s), Brighton ($TCNO_2$ ~5.0-6.0×10^{-5} moles/m^2, NO_x ~0.5-0.8 μg/m^2/s), Oxford ($TCNO_2$ ~7.0-7.5×10^{-5} moles/m^2, NO_x ~0.7-1.0 μg/m^2/s) and Chelmsford ($TCNO_2$ ~8.5-9.5×10^{-5} moles/m^2, NO_x ~0.5 μg/m^2/s). In northern England and the Midlands, peak $TCNO_2$ and NO_x emissions are located over Manchester ($TCNO_2$ ~10.0-11.0×10^{-5} moles/m^2, NO_x ~1.0-1.5 μg/m^2/s), Birmingham ($TCNO_2$ ~8.0-9.0×10^{-5} moles/m^2, NO_x ~1.0-1.5 μg/m^2/s), Leeds ($TCNO_2$ ~8.0-9.0×10^{-5} moles/m^2, NO_x ~1.0-1.5 μg/m^2/s) and Liverpool ($TCNO_2$ ~7.0-8.0×10^{-5} moles/m^2, NO_x ~0.5-1.0 μg/m^2/s).

To quantify the spatial relationship between the $TCNO_2$ and NO_x emissions over source regions, the corresponding pixels of both data sets were sub-sampled for each UK city (79 in total), normalised by the sample mean and correlated against each other (red circles, **Figure 4e**), which yielded a correlation $R_{city1x1}$ = 0.35 (i.e. city1×1 represents 1 grid box × 1 grid box or 0.025° × 0.025° around where the city centre is located). However, as atmospheric NO_2 is subject to chemical reactions and meteorological processes (e.g. transport), the signal around source regions is more diluted and the peak $TCNO_2$ not necessarily centred on the source. To allow for that, the spatial resolution of the quantities over each source was degraded, averaging over 3×3 (**Figure 4f**), 5×5 (**Figure 4g**) and 7×7 (**Figure 4h**) grid cells and the correlation recalculated (e.g. city3x3 represents 3 grid boxes × 3 grid boxes or 0.075° × 0.075° around where the city centre is located). This resulted in correlations of $R_{city3x3}$ = 0.53, $R_{city5x5}$ = 0.62 and $R_{city7x7}$ = 0.52. The correlation for full domain (i.e. the UK) was R_{all} = 0.20. As expected, the correlation for all grid pixels (e.g. including pixels over the sea) is weak where long-range transport of NO_2 can yield spatial variability in background regions with corresponding zero emission pixels. The $R_{city1x1}$, $R_{city3x3}$, $R_{city5x5}$ and $R_{city7x7}$ correlations were all larger. The largest city-scale correlation was for the $R_{city5x5}$ values where the spatial variability has been smoothed and is representative of the more diffuse pattern of $TCNO_2$. However, the $R_{city7x7}$ (0.175° × 0.175° or ~15-20 km × 15-20 km) correlation is lower than the $R_{city5x5}$ value suggesting that this scale is larger than most UK city sizes. Overall, for all R values, except for R_{all}, there are statistically significant positive correlations at the 90% confidence level (CL) or above (>95% CL for $R_{city3x3}$, $R_{city5x5}$ and $R_{city7x7}$). Therefore, the city-scale emission-satellite correlations provide confidence in the spatial distribution of the NAEI NO_x emissions based on the observed satellite $TCNO_2$.

3.2 Satellite NO_2 and Emission NO_x Trends

To evaluate the temporal evolution of the NAEI emissions, we use the long-term satellite record of $TCNO_2$ from OMI between 2005 and 2015. Annual total UK emissions of NO_x (expressed as NO_2 here) from the NAEI start in 1970 and continue to present day (typically with a lag of approximately two years). Annual spatial maps of the NAEI also exist over the same time period. However, while there is a consistent methodology for the UK total estimates, the mapping methodology updates between years (NAEI, 2017). Therefore, instead of performing trends on the maps, we focus on trends in the UK NO_x emission totals. For OMI, we have taken a similar broad scale approach focussing on averaged $TCNO_2$ across England (defined as 3°W-2°E, 50-54°N). We focus on England as the majority of large UK sources with reasonable spatiotemporal coverage are located here and have clearly defined trends over source regions. Pope et al., (2018) showed significantly (at the 95% CL) decreasing trends over London, Birmingham, Manchester and the Yorkshire power stations of between 1.5% and 2.3% per year. OMI measurements can be subject to large uncertainties and variability, so this analysis also investigates trends in a range of OMI $TCNO_2$ percentiles over time. To estimate the annual absolute England total NAEI NO_x emissions, we summed the emissions data for England (same geographical definition as for OMI above) from the 2019 NAEI NO_x emissions map and imposed the UK total NO_x trend on it. Here, we use a simple linear fit which yields an annual decrease in the UK total NO_x emission of 4.4%. The relative rate of change is the same for the England total NO_x emissions, but the absolute values are lower than the UK total NO_x emissions (**Figure 5, top panel**).

Over the 2005-2015 period, the England average OMI $TCNO_2$ trends in the 10th, 25th, 50th, 75th and 90th percentiles are -0.18 $\times10^{-5}$ moles/m^2/yr (-3.3%/yr), -0.20 $\times10^{-5}$ moles/m^2/yr (-2.7%/yr), -0.21 $\times10^{-5}$ moles/m^2/yr (-2.2%/yr), -0.17 $\times10^{-5}$ moles/m^2/yr (-1.3%/yr) and -0.07 $\times10^{-5}$ moles/m^2/yr (-0.4%/yr), respectively (**Figure 5**). All of the satellite trends are significant at the 95% CL except for the 90th percentile. The UK and England total NO_x emission trends between 2005 and 2015 are -76.3 kt/yr and -45.5 kt/yr (both -4.4%/yr). The OMI $TCNO_2$ trends range between -3.2% and -0.4% depending on the data percentile used to generate the average England $TCNO_2$ annual time series. We also calculated annual trends in UK and England (same definition as above) surface NO_2 observations (**Figure 5**, bottom panel) from AURN (AURN, 2021). Here, we used urban background, suburban and rural sites. For the 10th, 25th, 50th, 75th and 90th percentiles, UK (England) trends are -0.26 (-0.27) μg/m^3/yr, -0.40 (-0.52) μg/m^3/yr, -0.73 (-0.77) μg/m^3/yr, -0.95 (-0.95) μg/m^3/yr and -1.19 (-1.09) μg/m^3/yr. This corresponds to -3.77 (-3.03) %/yr, -3.07 (-3.24) %/yr, -3.03 (-2.86) %/yr, -2.49 (-2.31) %/yr and -2.29 (-1.98) %/yr. Therefore, the NAEI NO_x emissions trend is of similar magnitude and direction to that of the observations. The differences are most likely explained by the non-linear conversion of emissions to atmospheric concentrations (i.e. complex meteorology and chemistry). The likely drivers for decreases in UK NO_x emissions and NO_2 concentrations include a shift to cleaner energy sources (e.g. National Emissions Ceilings Regulations 2018, DEFRA. (2018b)), regulations on industrial and power generation emissions (Environmental Permitting Regulations 2016 (UK Government, 2016)) and tighter emissions for vehicles (e.g. Euro 6 emissions standards). Overall, these results provide confidence in the use of the satellite data as a tool to evaluate bottom-up emission trends.

3.3 Top-Down NO_x Emissions

The top-down NO_x emission rate for London under westerly flow (**Figure 2**) is 55.2 moles/s (37.7, 72.7 moles/s, i.e. satellite total error range), while the NAEI flux is 30.9 moles/s. Here, the NAEI has a low bias with the top-down estimate and sits outside the uncertainty range. The top-down emissions are based on 2 years, so the flux should be representative of an annual emission rate, corresponding to the NAEI reporting. In the case of Birmingham (**Figure 3a**), under easterly flow, there is a visible plume (i.e. positive differences of 2.0-3.0×10^{-5} moles/m^2) superimposed on a background enhancement (0.5-1.0×10^{-5} moles/m^2). As a result, the wind-flow *NO_2 LD* is always larger than the all-flow *NO_2 LD* and never reaches the background level (i.e. zero differences in **Figure 3a**) within the domain for which the TROPOMI $TCNO_2$ data has been processed for (e.g. there are positive differences in between the source, Birmingham, and the west of the domain, 8^{o}W). Therefore, the running t-test methodology is used to determine when the wind-flow *NO_2 LD* reaches a steady background state *B*, as shown in **Figure 3b**. Overall, the NAEI (12.9 moles/s) underestimates the top-down emissions for Birmingham under easterly flow (29.0 (17.7, 40.2) moles/s).

Our methodology was applied to 10 city sources where sources had suitable downwind $TCNO_2$ enhancements to derive *NO_2 LDs* and top-down emissions (**Figure 6**). A suitable downwind $TCNO_2$ enhancement was subjectively identified when a clear $TCNO_2$ enhancement (i.e. positive anomalies) under a specific wind flow/direction occurred and a realistic lifetime (i.e. in the range of the literature – e.g. Verstraeten et al. (2018)) could be derived from the downwind $TCNO_2$ profile of the target source. These are shown in **Table 1**. Where top-down emissions could be derived for sources over several wind directions, they were averaged together. The $TCNO_2$ response to mesoscale and synoptic weather systems (i.e. large scale flow) can be seasonally influenced (e.g. Pope et al., 2015) with some wind directions occurring more frequently in certain seasons. Therefore, top-down NO_x emission estimates derived from several wind directions for a particular source, though sampled throughout all months, can vary depending on the seasonal influence on the observed $TCNO_2$ for which the wind direction more frequently occurs in. The top-down emissions derived here suggest that the NAEI bottom-up emissions for the largest sources such as London and Birmingham are underestimated. The top-down emissions for London and Birmingham are 47.9 (31.2, 64.5) moles/s, and 22.1, (13.3, 30.9) moles/s with corresponding NAEI emissions of 30.9 moles and 12.9 moles/s, respectively. The NAEI (10.0 moles/s) also underestimates the emissions for Manchester 20.5 (3.3, 37.7) moles/s, but the top-down emission uncertainty is large (dominated by the smaller sample size of 29 days and large precision errors in the $TCNO_2$ data), so sits within its uncertainty range.

For the smaller sources (e.g. Edinburgh, Bristol, Cardiff, Leeds, Norwich and Belfast), the comparisons are in better agreement with the NAEI and are located within the top-down emission ranges. However, for Newcastle the NAEI emissions (3.1 moles/s) are substantially larger than the top-down estimate (1.7 (0.9, 2.3) moles/s). For the NO_2 effective lifetime, we find it ranges between 2.9 and 7.9 hours, which is consistent with values in the literature (e.g. Schaub et al., 2007; Pope et al., 2015), For all cities in **Figure 6** there is a strong correlation (0.99) between the NAEI and top-down emission sources investigated here, but the NAEI has a low bias of -4.18 moles/s (-37.4%) on average, dominated by the larger sources (i.e. London and Birmingham). These metrics were calculated in linear space.

4. Conclusions

We have evaluated relationships between satellite observations (TROPOspheric Monitoring Instrument, TROPOMI) of tropospheric column nitrogen dioxide ($TCNO_2$) and the UK National Atmospheric Emissions Inventory (NAEI) for nitrogen oxides ($NO_x = NO + NO_2$). Although they are different quantities, the short NO_2 lifetime means that our comparison can serve as a useful and important tool to evaluate bottom-up emissions. Here, spatial comparison of the TROPOMI $TCNO_2$ with the NAEI highlights consistency over the source regions with co-located peak values in the respective data sets. Correlation analysis of $TCNO_2$ and NO_x emissions over the UK cities indicates moderate spatial agreement with R ranging between 0.4 and 0.6 (significant at the >90% confidence level). Analysis of long-term satellite records of $TCNO_2$ (from the Ozone Monitoring Instrument (OMI), 2005-2015) show comparable negative trends with the NAEI NO_x emissions with rates of -2.2%/yr and -4.4%/yr, respectively. Though the relative NAEI trend is larger than OMI, meteorological conditions and photochemistry will control the atmospheric response to a change in NO_x emissions, as seen by OMI. It is also possible that the NAEI overestimates the decreasing NO_x emissions trend.

We have also used TROPOMI data to derive top-down city-scale estimates of UK NO_x emissions. While it can still be challenging to derive emissions from city scale sources (e.g. frequent cloud cover in the UK), we estimate top-down emissions fluxes (using satellite data between February 2018 and January 2020) for several cities. Most of the city sources show reasonable agreement, but for larger sources like London and Birmingham, the top-down emission values are substantially larger than those in the NAEI for 2019. Overall, as far as we are aware, this study represents the first robust attempt to use satellite observations of $TCNO_2$ to evaluate and constrain the official UK bottom-up NAEI. We find spatial and temporal agreement between the two quantities, but find evidence that the NAEI NO_x emissions for larger sources (e.g. London) may be too low (i.e. by >25%) sitting outside the top-down emission uncertainty ranges. To fully understand the discrepancies and the drivers of these NO_x emissions differences, further investigation is required.

Data Availability

TROPOMI and OMI tropospheric column NO_2 data comes from the Tropospheric Emissions Monitoring Internet Service (TEMIS, https://www.temis.nl/airpollution/no2.php). The bottom-up NO_x emissions come from the National Atmospheric Emissions Inventory (https://naei.beis.gov.uk/data/data-selector?view=air-pollutants) and the point and area sources can be obtained from https://naei.beis.gov.uk/data/map-uk-das?pollutant_id=6&emiss_maps_submit=naei-20210325121854. The specific UK total NO_x emissions came from https://naei.beis.gov.uk/data/data-selector-results?q=142818. Meteorological wind, temperature and boundary layer height data came from ECMWF (https://cds.climate.copernicus.eu/cdsapp#!/dataset/reanalysis-era5-pressure-levels?tab=overview). CAMS NO_2 data was retrieved form https://ads.atmosphere.copernicus.eu/cdsapp#!/dataset/cams-global-reanalysis-eac4?tab=form.The AURN data was obtained from https://uk-air.defra.gov.uk/networks/network-info?view=aurn.

Author contribution

RJP undertook the research looking at the spatial maps and long-term trends. RJP, RK, CW and AMG worked on the satellite top-down city-scale NO_x emission estimates. RJP prepared the manuscript with contributions from all co-authors.

Competing interests

The authors declare that they have no conflict of interest.

Acknowledgements

This work was funded by the Department for Environment, Food and Rural Affairs Affairs through the “Applying Earth Observation (EO) to Reduce Uncertainties in Emission Inventories” project and by the UK Natural Environment Research Council (NERC) by providing funding for the National Centre for Earth Observation (NCEO, award reference NE/R016518/1).

References

AURN. Automated Urban and Rural Network [Online]. Available: https://uk-air.defra.gov.uk/networks/network-info?view=aurn (accessed 30th March 2021), 2021.

Beirle, S., Boersma, B.F., Platt, U., Lawrence, M.G. and Wagner, T.: Megacity emissions and lifetimes of nitrogen oxides probed from space, *Science*, 333, 1737, doi:10.1126/science.1207824, 2011.

Boersma, K.F., Eskes, H.J., Veefkind, J.P., Brinksma, E.J., van der A, R.J., Sneep, M., van den Oord, G.H.J., Levelt, P.F., Stammes, P., Gleason, J.F. and Bucsela, E.J.: Near-real time retrieval of tropospheric NO_2 from OMI, *Atmospheric Chemistry and Physics*, 7, 2103–2118, doi:10.5194/acp-7-2103-2007, 2007.

Braak R. 2010. Row Anomaly Flagging Rules Lookup Table, KNMI Technical Document TN-OMIE-KNMI-950, *KNMI*, Netherlands.

CAMS. CAMS global reanalysis (EAC4). Available: https://ads.atmosphere.copernicus.eu/cdsapp#!/dataset/cams-global-reanalysis-eac4?tab=form (accessed 29th November 2021), 2021.

Chan, K. L., Wiegner, M., van Geffen, J., De Smedt, I., Alberti, C., Cheng, Z., Ye, S. and Wenig, M.: MAX-DOAS measurements of tropospheric NO_2 and HCHO in Munich and the comparison to OMI and TROPOMI satellite observations, *Atmospheric Measurement Techniques*, 13, 4499–4520, doi: 10.5194/amt-13-4499-2020, 2020.

DEFRA. Air Pollution in the UK 2017 [Online]. Available: https://uk-air.defra.gov.uk/assets/documents/annualreport/air_pollution_uk_2017_issue_1.pdf (last accessed 30th March 2021), 2018a.

DEFRA. UK Informative Inventory Report (1990 to 2016) [Online]. Available: https://uk-air.defra.gov.uk/library/reports?report_id=956 (last accessed 30th March 2021), 2018b.

DEFRA. Air Pollution in the UK 2019 [Online]. Available: https://uk-air.defra.gov.uk/library/annualreport/viewonline?year=2019_issue_1#report_pdf (accessed 30th March 2021), 2020.

Dibbens, C. and Clemens, T.: Place of work and residential exposure to ambient air pollution and birth outcomes in Scotland, using geographically fine pollution climate mapping estimates, *Environmental Research*, 140, 535-541, doi:10.1016/j.envres.2015.05.010, (2015).

Dimitropoulou, E., Hendrick, F., Pinardi, G., Friedrich, M. M., Merlaud, A., Tack, F., De Loungeville, H., Fayt, C., Hermans, C., Laffineur, Q., Fierens, F. and Van Roozendael, M.: Validation of TROPOMI tropospheric NO_2 columns using dual-scan multi-axis differential optical absorption spectroscopy (MAX-DOAS) measurements in Uccle, Brussels, *Atmospheric Measurement Techniques*, 13, 5165–5191, doi: 10.5194/amt-13-5165-2020, 2020.

ECMWF. ERA5 hourly data on pressure levels from 1979 to present. Available at: https://cds.climate.copernicus.eu/cdsapp#!/dataset/reanalysis-era5-pressure-levels?tab=overview (accessed 29th November 2021), 2021.

EEA. Air quality in Europe — 2018 report [Online]. Available: https://www.eea.europa.eu/publications/air-quality-in-europe-2018 (accessed 30th March 2021), 2018.

EMEP/EAA. EMEP/EEA air pollutant emission inventory guidebook 2019, EEA Report No 13/2019, ISSN 1977-8449. Available: https://www.eea.europa.eu/publications/emep-eea-guidebook-2019 (accessed 2nd July 2021), 2019.

EMEP. EMEP – Convention on Long-range Transboundary Air Pollution. Available: https://www.emep.int/ (accessed 12th July 2021), 2021.

Liu, F., Beirle, S., Zhang, Q., Dörner, S., He, K. and Wagner T.: NOx lifetimes and emissions of cities and power plants in polluted background estimated by satellite observations, *Atmospheric Chemistry and Physics,* 16, 5283-5298, doi:10.5194/acp-16-5283-2016, 2016.

Martin, R.V., Jacob, D.J., Chance, K., Kurosu, T.P., Palmer, P.I. and Evans, M.J.: Global inventory of nitrogen oxide emissions constrained by space-based observations of NO_2 columns, *Journal of Geophysical Research,* 108, 4537, doi:10.1029/2003JD003453, 2003.

Miyazaki, K., Eskes, H., Sudo, K., Boersma, K.F., Bowman, K. and Kanaya, Y.: Decadal changes in global surface NO_x emissions from multi-consistent satellite data assimilation, *Atmospheric Chemistry and Physics,* 17, 807-837, doi:10.5194/acp-17-807-2017, 2016.

NAEI. UK Emission Mapping Methodology. – 2015 [Online]. Available: https://uk-air.defra.gov.uk/assets/documents/reports/cat07/1710261436_Methodology_for_NAEI_2017.pdf (accessed 30th March 2021), 2017.

NAEI. UK-NAEI – National Atmospheric Emissions Inventory [Online]. Available: https://naei.beis.gov.uk/ (accessed 30th March 2021), 2021.

Pena-Angulo, D., Reig-Gracia, F., Dominguez-Castro, F., Revuelto, J., Aguilar, E., van der Schrier, G. and Vicente-Serrano, S. M.: ECTACI: European Climatology and Trends Atlas of Climate Indices (1979-2017), *Journal of Geophysical Research: Atmospheres*, 125, e2020JD032798, doi: 10.1029/2020JD032798, 2020. Pope, R.J., Savage, N.H., Chipperfield, M.P., Ordonez, C. and Neal, L.S.: The influence of synoptic weather regimes on UK air quality: Regional model studies of tropospheric column NO_2, *Atmospheric Chemistry and Physics,* 15, 11201-11215, doi:10.5194/acp-15-11201-2015, 2015.

Pope, R.J., Arnold, S.R., Chipperfield, M.P., Latter, B.G., Siddans, R. and Kerridge, B.J.: Widespread changes in UK air quality observed from space, *Atmospheric Science Letters,* 19, e817, doi: 10.1002/asl.817, 2018.

Potts, D.A., Marais, E.A., Boesch, H., Pope, R.J., Lee, J., Drysdale, W., Chipperfield, M.P., Kerridge, B. and Siddans, R.: Diagnosing air quality changes in the UK during the COVID-19 lockdown using TROPOMI and GEOS-Chem, *Environmental Research Letters,* 16, 054031, doi:10.1088/1748-9326/abde5d, 2021.

Ricardo Energy and Environment. UK Informative Inventory Report (1990 to 2019). Available: https://uk-air.defra.gov.uk/assets/documents/reports/cat09/2103151107_GB_IIR_2021_FINAL.pdf (accessed 2nd July 2021), 2021.

Royal College of Physicians. Every breath we take: the lifelong impact of air pollution [Online]. Available: https://www.rcplondon.ac.uk/projects/outputs/every-breath-we-take-lifelong-impact-air-pollution (accessed 30th March 2021), 2016.

Savage, N.H., Agnew, P., Davis, L.S., Ordóñez, C., Thorpe, R., Johnson, C.E., O'Connor, F.M. and Dalvi, M.: Air quality modelling using the Met Office Unified Model (AQUM OS24-26): model description and initial evaluation, *Geoscientific Model Development,* 6, 353–372, doi:10.5194/gmd-6-353-2013, 2013.

Schaub, D., Brunner, D., Boersma, K.F., Keller, J., Folini, D., Buchmann, B., Berresheim, H. and Staehelin, J.: SCIAMACHY tropospheric NO_2 over Switzerland: estimates of NOx lifetime and impacts of the complex alpine topography on the retrieval, *Atmospheric Chemistry and Physics,* 7, 5971-5987, doi:10.5194/acp-7-5971-2007, 2007.

Seinfeld, J. and Pandis, S.: Atmospheric Chemistry and Physics: From Air Pollution to Climate Change - Second Edition, John Wiley and Sons Inc, New Jersey, USA, 2006.

Torres, O., Bhartia, P. K., Jethva, H. and Ahn, C.: Impact of the ozone monitoring instrument row anomaly on the long-term record of aerosol products, *Atmospheric Measurement Techniques*, 11, 2701-2715, doi:10.5194/amt-11-2701-2018, 2018.

Tsagatakis, I., Richardson, J., Evangelides, C., Pizzolato, M., Pearson, B., Passant, N., Pommier, M. and Otto, A.: UK Spatial Emissions Methodology: A report of the National Atmospheric Emission Inventory 2019. Available at: https://uk-air.defra.gov.uk/assets/documents/reports/cat09/2107291052_UK_Spatial_Emissions_Methodology_for_NAEI_2019_v1.pdf (accessed 29th November 2021), 2021.

UK Government. The Environmental Permitting (England and Wales) Regulations 2016. Available: https://www.legislation.gov.uk/uksi/2016/1154/contents/made (last accessed 2nd July 2021), 2016.

Veefkind, J.P., Aben, I., McMullan, K., Forster, H., de Vries, J., Otter, G., Claas, J., Eskes, H.J., de Haan, F., Kleipool, Q., van Weele, M., Hasekamp, O., Hoogeveen, R., Landgraf, J., Snel, R., Tol, P., Ingmann, P., Voors, R., Kruizinga, B., Vink, R., Visser, H. and Levelt, P.F.: TROPOMI on the ESA Sentinel-5 Precursor: A GMES mission for global observations of atmospheric composition for climate, air quality and ozone layer applications, *Remote Sensing of Environment,* 120, 70-83, doi:10.1016/j.rse.2011.09.027, 2012.

Verhoelst, T., Compernolle, S., Pinardi, G., Lambert, J. C., Eskes, H., Eichmann, K. U., et al.: Ground-based validation of the Copernicus Sentinel-5P TROPOMI NO2 measurements with the NDACC ZSL-DOAS, MAX-DOAS and Pandonia global networks, *Atmospheric Measurement Techniques*, 14, 481–510, doi: 10.5194/amt-14-481-2021, 2021.

Verstraeten, W.W., Boersma, K.F., Douros, J., Williams, J.E., Eskes, H., Liu, F., Beirle, S. and Delcloo, A.: Top-down NO_x emissions of European cities based on the downwind plume of modelled and space-borne tropospheric NO_2 column, *Sensors,* 18 (9), 2893, doi:10.3390/s18092893, 2018.

WHO. Ambient (outdoor) air pollution [Online]. Available: https://www.who.int/news-room/fact-sheets/detail/ambient-(outdoor)-air-quality-and-health (last accessed 30th March 2021), 2018.

Wu, H., Reis, S., Lin, C. and Heal, M.R.: Effect of monitoring network design on land use regression models for estimating residential NO_2 concentration, *Atmospheric Environment,* 149, 24-33, doi:10.1016/j.atmosenv.2016.11.014, 2017.

Figures

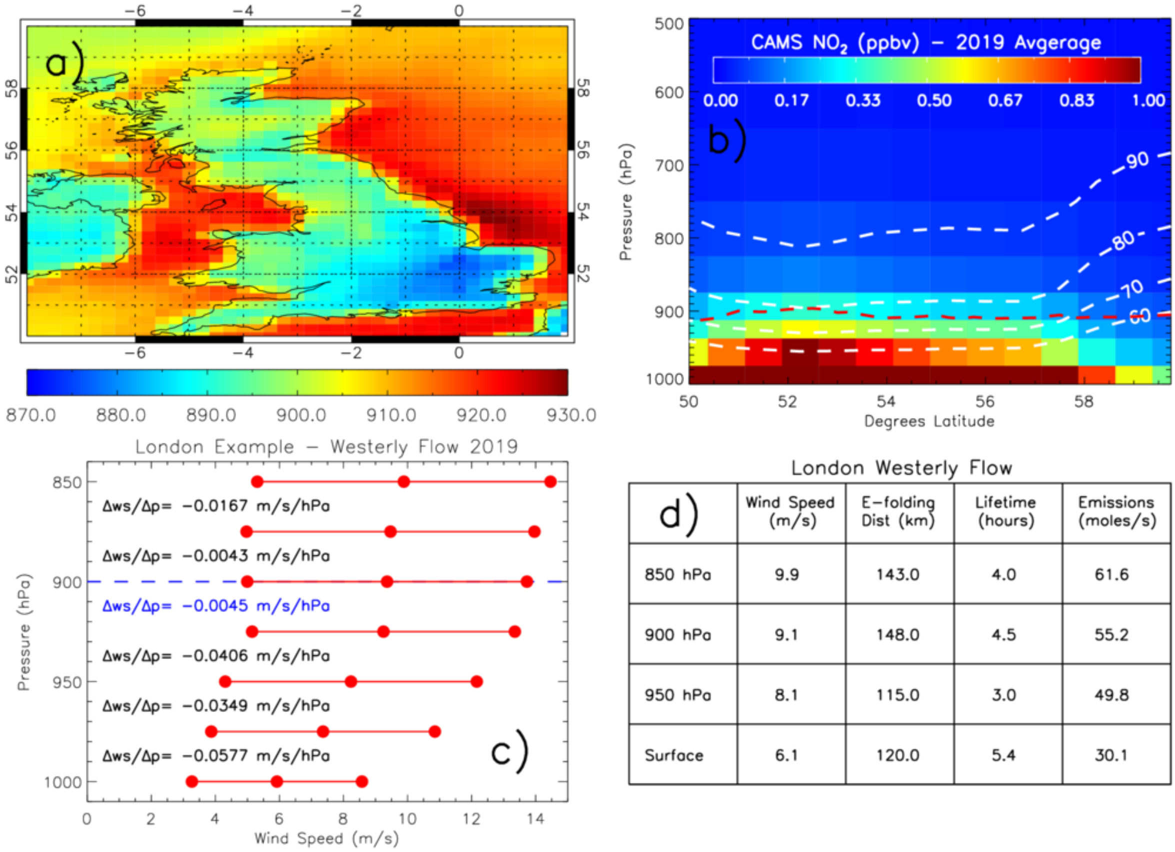

d)	Wind Speed (m/s)	E−folding Dist (km)	Lifetime (hours)	Emissions (moles/s)
850 hPa	9.9	143.0	4.0	61.6
900 hPa	9.1	148.0	4.5	55.2
950 hPa	8.1	115.0	3.0	49.8
Surface	6.1	120.0	5.4	30.1

Figure 1: *a) ERA-5 UK boundary layer pressure (hPa) sampled at 13.00 LT (to coincide with the TROPOMI overpass time) and averaged for 2019. b) CAMS reanalysis zonal (8.0°W-2.0°E) average latitude-pressure NO_2 (ppbv) cross-section over the UK between the surface and 500 hPa. White dashed lines represent the percentage of the surface-500 hPa NO_2 loading between the surface and the respective pressure levels. The red dashed line represents the zonal average boundary layer pressure (hPa). c) Average (surface to pressure level) wind speed (m/s), ± the standard deviation, profile over London under westerly flow (determined from the ERA-5 u-wind and v-wind components at each pressure level). Δws/Δp is the wind speed gradient between pressure levels. The blue text indicates the first small step change in the gradient indicative of reduced flow turbulence and a suitable surface-altitude range to average the winds speeds over. d) The table shows the impact to the NO_x emission parameters when using different altitudes over which to average the wind speeds.*

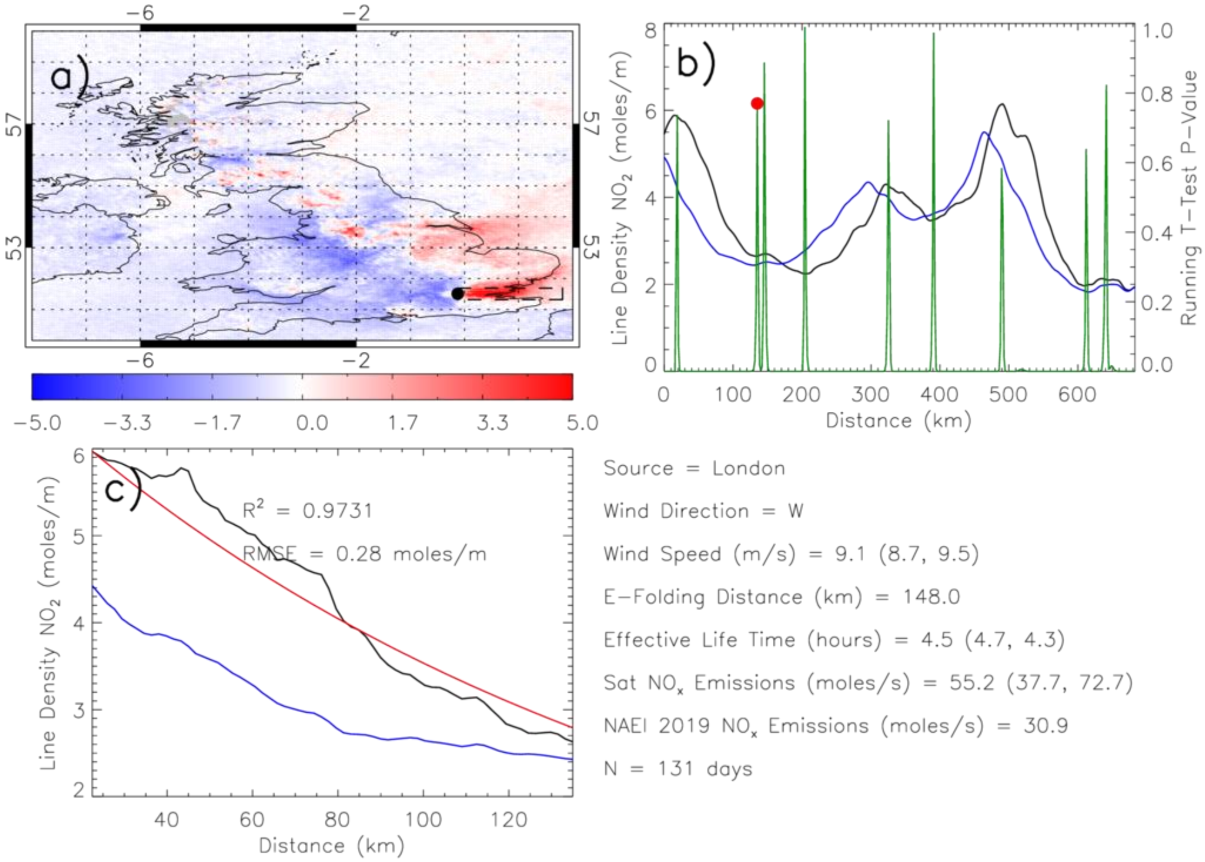

Figure 2: *(a) TROPOMI TCNO$_2$ (10^{-5} moles/m^2) sub-sampled under westerly flow (defined over London, black dot) minus the long-term average (February 2018 to January 2020). The dashed box represents the width of the source and distance between the source and background. (b) Downwind NO$_2$ LD from London (black = westerly flow, blue = all-flow average) with the corresponding running t-test p-value (green line). The red dot represents the location of background level determined by the turning point in the running t-test p-value time series. (c) The westerly flow and all-flow NO$_2$ LD between peak westerly flow NO$_2$ LD and the background value. The red line represents the e-folding distance fit with the corresponding R^2 and root mean square error (RMSE) between the westerly flow NO$_2$ LD and fit profile. N represents the number of days classified under westerly flow over London.*

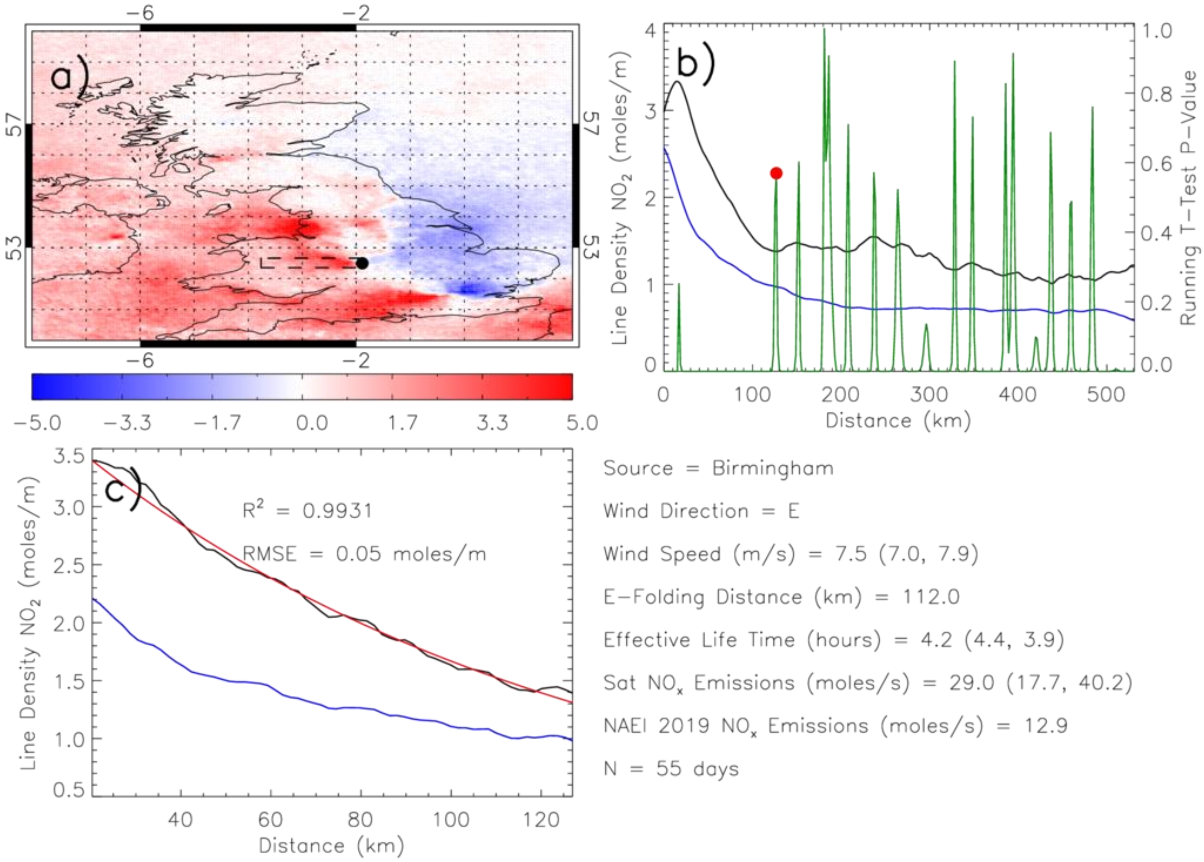

Figure 3: *(a) TROPOMI $TCNO_2$ (10^{-5} moles/m^2) sub-sampled under easterly flow (defined over Birmingham, black dot) minus the long-term average (February 2018 to January 2020). The dashed box represents the width of the source and distance between the source and background. (b) Downwind NO_2 LD from Birmingham (black = easterly flow, blue = all-flow average) with the corresponding running t-test p-value (green line). The red dot represents the location of background level determined by the turning point in the running t-test p-value time series. (c) The easterly flow and all-flow NO_2 LD between peak easterly flow NO_2 LD and the background value. The red line represents the e-folding distance fit with the corresponding R^2 and root mean square error (RMSE) between the easterly flow NO_2 LD and fit profiles. N represents the number of days classified under easterly flow over Birmingham.*

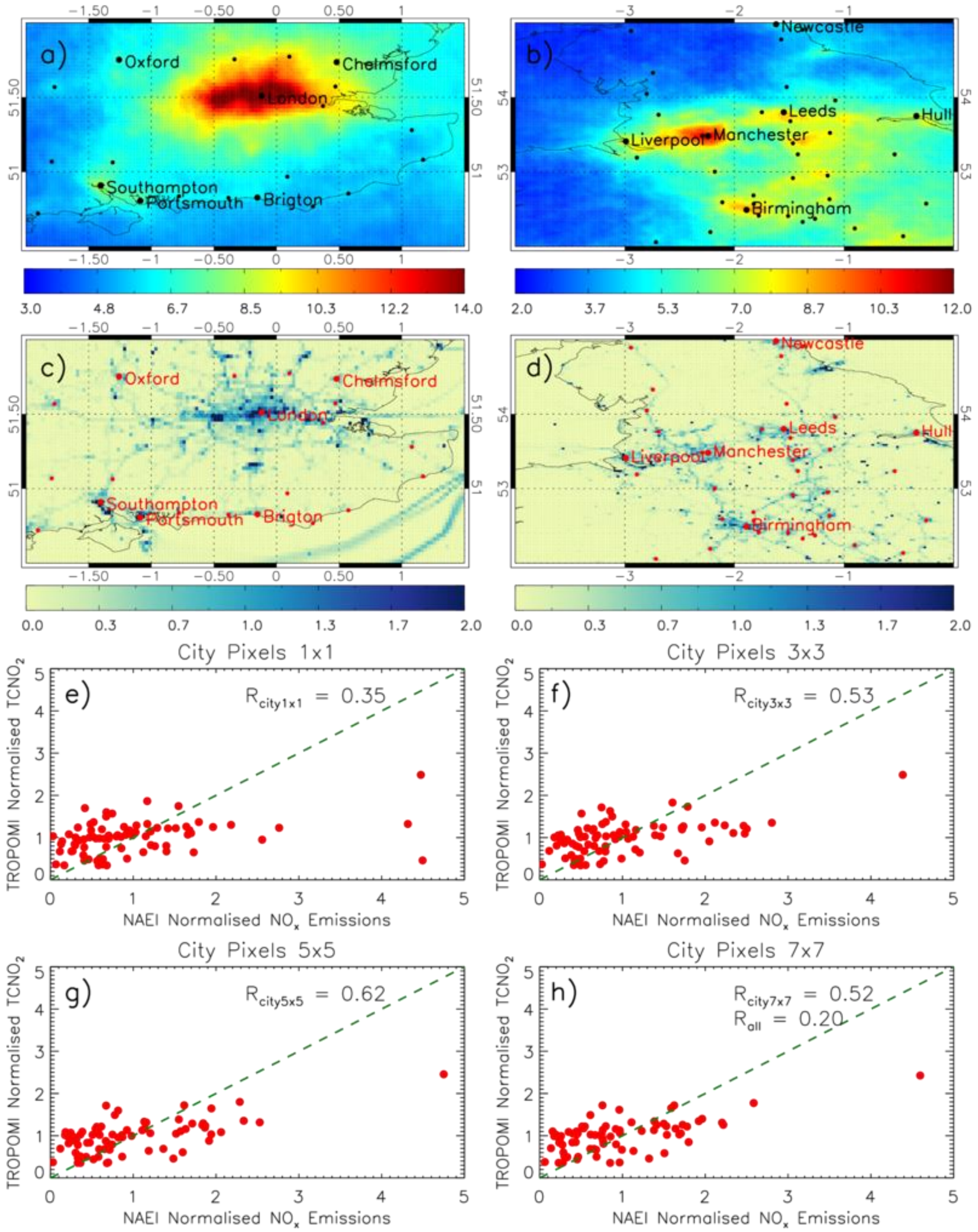

Figure 4: *TROPOMI $TCNO_2$ ($\times10^{-5}$ moles/m^2) average for February 2018 to January 2020 across (a) south-eastern and (b) northern England. Black circles represent city locations. NAEI NO_x emissions (µg/m^2/s) for 2019 across (c) south-eastern and (d) northern England. Red circles represent city locations. Panels (e)-(h) represent the correlation of normalised $TCNO_2$ and NO_x emissions for UK cities. The green dashed line is the 1:1 line. Each source is normalised by the average of all the sources. The four panels also represent city means using*

varying pixel ranges around the source (i.e. 1×1, 3×3, 5×5 and 7×7 grid pixels). The correlations between the city-scale normalised NO_x emissions and $TCNO_2$ are shown (R).

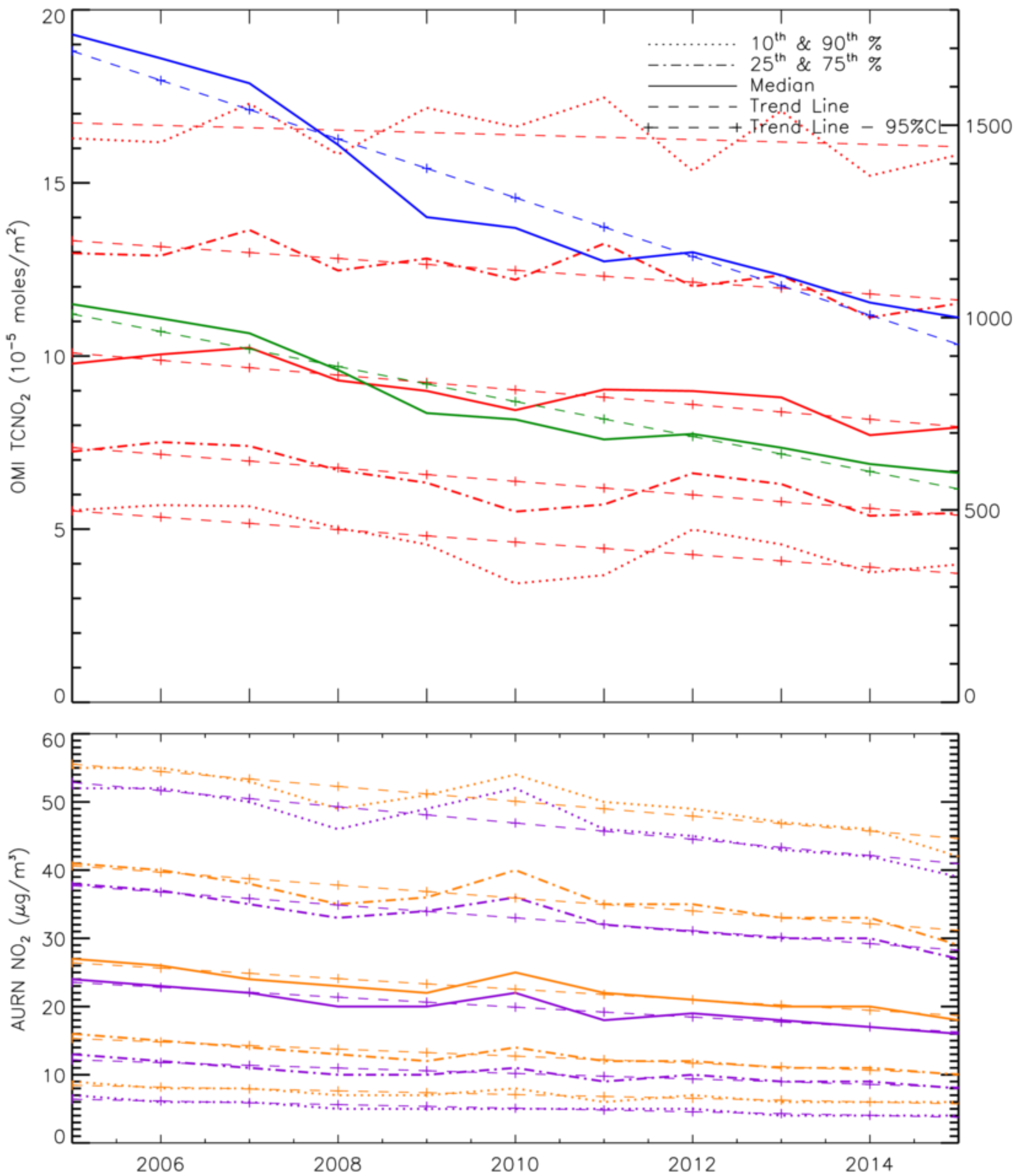

Figure 5: *The top panel shows time series (2005 to 2015) in OMI $TCNO_2$ ($\times 10^{-5}$ moles/m^2) and NAEI NO_x emission totals (kt or Gg). OMI median, 10^{th} & 90^{th} and 25^{th} & 75^{th} percentiles are represented by solid, dotted and dot-dashed lines, respectively. NAEI NO_x emission totals for the UK and England are represented by the blue and green solid lines. Here, the OMI $TCNO_2$ has been averaged over England (defined as 3°W-2°E, 50-54°N) and while the UK NO_x emission totals are directly reported by the NAEI, the England NO_x emission totals have been summed over the emissions maps for the same England definition used for OMI (see Section 3.2 for more information).* In the bottom panel, *AURN surface NO_2 ($\mu g/m^3$) times series are shown for the UK (purple) and England (orange).* Trends lines are shown by dashed and dash-crossed lines for insignificant and significant trends (at the 95% confidence level).

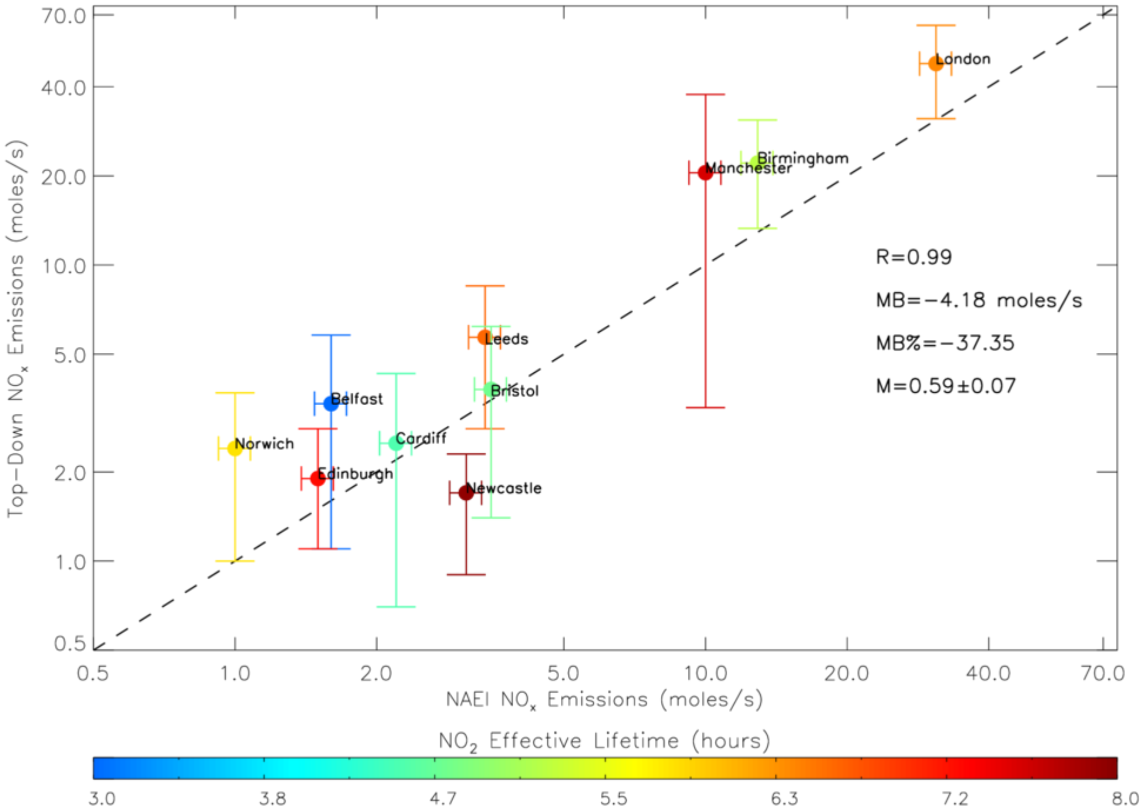

Figure 6: *NAEI and top-down (TROPOMI) NO_x emissions (moles/s) for 10 UK cities coloured by the NO_2 effective lifetime (hours). Where there is more than one top-down estimate for a city from multiple wind directions, the corresponding emission rates and lifetimes have been averaged together. The correlation (R), mean bias (MB, moles/s, i.e. NAEI-top down), percentage mean bias (MB%) and linear fit (M, i.e. top down vs. NAEI) are also shown. NAEI uncertainty is ±7.8% (DEFRA, 2018b) and the top-down uncertainty range is based on satellite errors. The black dashed line represents the 1:1 relationship and both axes are on log scales.*

Table 1: *List of top-down NO_x (moles/s) emission estimates for UK city sources under different wind directions. The Sat NO_x Emissions lower and upper ranges represent the emission flux ± the total error.*

Source Name	London	London	London	Birmingham
Longitude	-0.13	-0.13	-0.13	-1.89
Latitude	51.51	51.51	51.51	52.50
Lon Edge - West	-0.52	-0.52	-0.52	-2.18
Lon Edge - East	0.28	0.28	0.28	-1.72
Lat Edge - South	51.32	51.32	51.32	52.35
Lat Edge - North	51.69	51.69	51.69	52.66
Wind Speed Average (m/s)	9.10	7.00	7.50	7.50
Wind Speed Standard Error (m/s)	0.40	0.50	0.40	0.50
Wind Direction	W	N	E	E
E-Folding Distance (km)	148.00	189.00	195.00	112.00
Life Time (hr)	4.50	7.50	7.20	4.20
Life Time- Lower Wind (hr)	4.70	8.10	7.60	4.40
Life Time- Upper Wind (hr)	4.30	7.10	6.80	3.90
Satellite Emission Rate (moles/s)	55.20	55.90	32.50	29.00
Sat NOx Emissions - Lower (moles/s)	33.90	33.9	22.00	17.70
Sat NOx Emissions - Upper (moles/s)	72.7	77.8	42.90	40.20
NAEI Emission Rate (moles/s)	30.90	30.90	30.90	12.90
Number of Days	131	53	54	55

Source Name	Birmingham	Birmingham	Newcastle	Manchester
Longitude	-1.89	-1.89	-1.62	-2.25
Latitude	52.50	52.50	54.98	53.50
Lon Edge - West	-2.18	-2.18	-1.73	-2.47
Lon Edge - East	-1.72	-1.72	-1.40	-2.01
Lat Edge - South	52.35	52.35	54.92	53.37
Lat Edge - North	52.66	52.66	55.02	53.60
Wind Speed Average (m/s)	5.80	9.10	10.50	5.60
Wind Speed Standard Error (m/s)	0.30	0.40	0.30	0.40
Wind Direction	N	S	W	N
E-Folding Distance (km)	184.00	91.00	297.00	152.00
Life Time (hr)	8.70	2.80	7.90	7.50
Life Time- Lower Wind (hr)	9.40	2.90	8.10	8.20
Life Time- Upper Wind (hr)	8.20	2.60	7.60	6.90
Satellite Emission Rate (moles/s)	12.20	25.20	1.70	20.5
Sat NOx Emissions - Lower (moles/s)	5.80	16.50	0.90	3.30
Sat NOx Emissions - Upper (moles/s)	18.70	33.90	2.30	37.7
NAEI Emission Rate (moles/s)	12.90	12.90	3.10	10.00
Number of Days	46	100	157	29

Source Name	Belfast	Edinburgh	Norwich	Cardiff
Longitude	-5.93	-3.19	1.29	-3.18
Latitude	54.61	55.96	52.63	51.49
Lon Edge - West	-6.00	-3.32	1.20	-3.36
Lon Edge - East	-5.84	-3.10	1.38	-3.10
Lat Edge - South	54.55	55.89	52.60	51.45
Lat Edge - North	54.70	55.98	52.69	51.55
Wind Speed Average (m/s)	8.30	10.10	10.30	5.30
Wind Speed Standard Error (m/s)	0.60	0.30	0.40	0.40
Wind Direction	E	W	W	N
E-Folding Distance (km)	87.00	262.00	214.00	86.00
Life Time (hr)	2.90	7.20	5.80	4.50
Life Time- Lower Wind (hr)	3.10	7.40	6.10	4.90
Life Time- Upper Wind (hr)	2.70	7.00	5.60	4.20
Satellite Emission Rate (moles/s)	3.40	1.90	2.40	2.50
Sat NOx Emissions - Lower (moles/s)	1.10	1.10	1.00	0.70
Sat NOx Emissions - Upper (moles/s)	5.80	2.80	3.70	4.30
NAEI Emission Rate (moles/s)	1.60	1.50	1.00	2.20
Number of Days	47	187	122	37

Source Name	Leeds	Bristol
Longitude	-1.55	-2.59
Latitude	53.80	51.46
Lon Edge - West	-1.69	-2.74
Lon Edge - East	-1.44	-2.47
Lat Edge - South	53.74	51.40
Lat Edge - North	53.86	51.55
Wind Speed Average (m/s)	8.70	7.20
Wind Speed Standard Error (m/s)	0.50	0.40
Wind Direction	S	E
E-Folding Distance (km)	207.00	123.00
Life Time (hr)	6.60	4.70
Life Time- Lower Wind (hr)	7.00	5.10
Life Time- Upper Wind (hr)	6.30	4.50
Satellite Emission Rate (moles/s)	5.70	3.80
Sat NOx Emissions - Lower (moles/s)	2.80	1.40
Sat NOx Emissions - Upper (moles/s)	8.50	6.20
NAEI Emission Rate (moles/s)	3.40	3.50
Number of Days	81	55